This article has been accepted for publication in a future issue of this journal, but has not been fully edited. Content may change prior to final publication.
Citation information: DOI: 10.17775/CSEEJPES.2021.03870, CSEE Journal of Power and Energy Systems

A Residue Based Open-loop Modal Analysis Method for Detecting LFMR of PMSG-WFs Penetrated Power Systems

Luonan Qiu, Tianhao Wen, Yang Liu, Q. H. Wu, Fellow, IEEE

Abstract—This paper proposes a residue based open-loop modal analysis method to detect the low frequency modal resonance(LFMR), including asymmetric low frequency modal attraction(ALFMA) and asymmetric low frequency modal repulsion(ALFMR), of permanent magnetic synchronous generator based wind farms(PMSG-WFs) penetrated power systems. The formation of ALFMA and ALFMR caused by two open-loop low frequency oscillation(LFO) modes moving close and apart is analyzed in detail. And, via predicting the trajectories of closed-loop LFO modes based on calculation of residue of open-loop LFO modes, both ALFMA and ALFMR can be detected. The proposed method can select LFO modes which move to the right half complex plane as control parameters vary. Simulation studies are carried out on a three-machine power system and the 4-machine 11-bus power system to verify the properties of the proposed method.

Index Terms—Low frequency modal resonance, residue based open-loop modal analysis method, asymmetric low frequency modal attraction, asymmetric low frequency modal repulsion

I. Introduction

In recent years, large-scale wind power plants have been increasingly integrated into power systems. But due to their basic operation principle and control strategies, they may cause low frequency oscillations(LFO), e.g., low frequency modal resonance(LFMR) in power systems. LFMR is worthy of being analyzed for it greatly affects the stable operation and power quality of power system [1].

The phenomenon of LFMR caused by near strong modal resonance, which is a mathematical concept in the theory of eigenvalue sensitivity [2], has been studied in [3]. In [3], Dobson used 3-bus system and 9-bus system to verify the existence of LFMR in power system. Besides, low frequency modal repulsion, a type of LFMR, was studied in [4] in detial. According to [4], low frequency modal repulsion can be caused by the interaction between open-loop converter oscillation mode (COM) of PMSG and open-loop electromechanical oscillation mode(EOM) of power system. Simulation studies in [4] indicated that low frequency modal repulsion may excite significant oscillation in power angle of synchronous generator.

So far, methods for investigation of LFMR between PMSG and the rest of power system include modal analysis, damping torque analysis, open-loop analysis method.Modal analysis is a widely applied method of studying LFMR of power system [5], [6]. The method consists of two steps. Firstly, the state equation of power system is linearized at the operating point to get the state matrix [7]. Secondly, by calculating the eigenvalues and eigenvectors of the state matrix, relevant information about LFMR can be obtained [8]. However, modal analysis can only judge the stability of power system near the operating point. Further information, such as the location of oscillation source, cannot be obtained. Moreover, due to the high dimension of the state matrix, it may take a long time for the method to perform stability analysis.

In addition, damping torque analysis(DTA) can also be used to study LFMR of power system. DTA was originally proposed in [9] for single-machine infinite-bus(SMIB) power system. In that paper, the influence of excitation controller on small-signal stability of the SMIB system is studied based on the Phillips-Herffron model. According to the Phillips-Herffron model, the disturbance of electromagnetic torque of synchronous generator, influenced by excitation controller, can be decomposed into synchronous torque proportional to the disturbance of rotor angle, and damping torque proportional to the difference between rotor speed and synchronous speed. The sign and magnitude of damping torque directly affect the LFO. As for the SMIB system, by calculating the part of damping torque associated with excitation control loop, the influence of excitation controller on small-signal stability can be directly judged [10]. When applied to analyze the stability of SMIB system, DTA method has a clear physical meaning and is easy to be understood. However, its physical meaning becomes obscure if it is used for judging the stability of multi-machine power system. And, it cannot find the exact location of LFO modes on the complex plane.

This work was supported in part by the State Key Program of National Natural Science Foundation of China under Grant No. U1866210, the National Natural Science Foundation of China under Grant No. 51807067 (Corresponding author: Yang Liu email: epyangliu@scut.edu.cn).

The authors are with the School of Electric Power Engineering, South China University of Technology, Guangzhou, 510640, China.

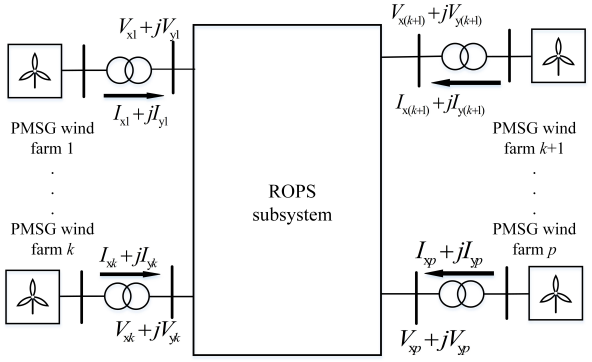

Fig. 1 A multi-machine power system with p PMSG wind farms

Recently, other methods of studying LFMR have been put forward, including the open-loop modal analysis method stated in [11]. The open-loop modal analysis method identifies any pair of open-loop LFO modes close to each other from two open-loop subsystems. And, an index, the indicator of the strength of symmetric modal repulsion of the identified open-loop modes, is calculated without the information of closed-loop eigenvalues. However, the method is only suitable for analyzing symmetric modal resonance. In particular, the location of closed-loop LFO modes and small-signal stability margin it gives are correct only when the identified pair of open-loop modes are equal. Besides, the mechanism of LFMR, especially ALFMA and ALFMR, has not been intensively analyzed in [4], [11], [12] or other papers.

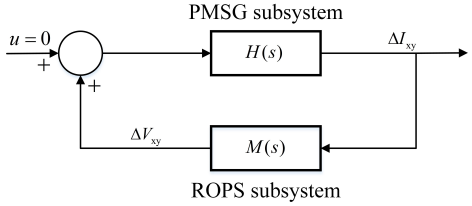

Fig. 2 Closed-loop model for calculation of residue of open-loop modes of PMSG subsystem

In this paper, first of all, a model for analyzing LFMR of PMSG-WFs integrated power system has been derived. The model consists of PMSG subsystem and the-rest-of-power-system(ROPS) subsystem. Then, the mechanism of ALFMA and ALFMR in PMSG-WFs integrated power system resulted from the interaction of open-loop LFO modes in PMSG subsystem and ROPS subsystem is analyzed. Furthermore, a residue based open-loop modal analysis method is proposed to detect ALFMA and ALFMR by estimating the trajectories of selected closed-loop LFO modes of the entire power system.

Compared with the open-loop modal analysis method proposed in [11], the method proposed in this paper has the following advantages

1) The proposed method can estimate the locations of closed-loop LFO modes more accurately no matter how close the interacting open-loop LFO modes are.
2) The proposed method can give more accurate small-signal stability margin, especially when ALFMA is encountered.

Besides, the error of estimation of the location of closed-loop LFO modes given by the proposed method is analyzed.

Two example PMSG-WFs integrated power systems are used to demonstrate the performances of the proposed method. The first example is a modified three-machine power system used for studying ALFMA, while the second example is a 4-machine 11-bus power system used for analyzing ALFMR.

II. ALFMA and ALFMR Caused By PMSG

A. A Closed-Loop Model of PMSG-WFs Integrated Power System for Analyzing LFMR

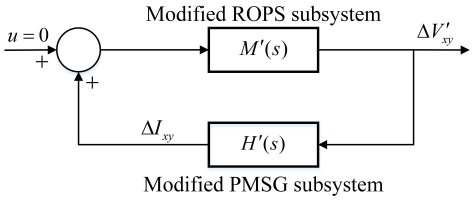

Fig. 3 Closed-loop model for calculation of residue of open-loop modes of ROPS subsystem

Fig. 1 shows a multi-machine power system with p PMSG-WFs, where $I_{\mathrm{x}k}+jI_{\mathrm{y}k}(k=1,2,\ldots,p)$ represents the output current of the kth PMSG-WFs and $V_{\mathrm{x}k}+jV_{\mathrm{y}k}(k=1,2,\ldots,p)$ represents the voltage at the point of common coupling(PCC) of the kth PMSG-WF, expressed in the common x-y coordinate of the power system. The system can be partitioned into PMSG subsystem and ROPS subsystem. As for PMSG subsystem, its linearized state-space model is

$$\begin{cases}\dfrac{\mathrm{d}}{\mathrm{d}t}\Delta\mathrm{X_w}=\mathrm{A_w}\Delta\mathrm{X_w}+\mathrm{B_w}\Delta\mathrm{V_{xy}}\\ \Delta I_{\mathrm{xy}}=\mathrm{C_w}\Delta\mathrm{X_w}\end{cases}\tag{1}$$

where

$$\mathrm{A_w}=\begin{pmatrix}\mathrm{A_{w1}} & 0 & \cdots & \cdots & \cdots & 0\\ 0 & \mathrm{A_{w2}} & 0 & & & \vdots\\ \vdots & 0 & \ddots & & & \vdots\\ \vdots & & & \mathrm{A_{w}}k & & \vdots\\ \vdots & & & & \ddots & 0\\ 0 & \cdots & \cdots & \cdots & 0 & \mathrm{A_{w}}p\end{pmatrix}$$

$\mathrm{A_w}k$ is the state matrix of the kth PMSG-WF, $\mathrm{X_w}$ is the vector of all the state variables of p PMSG-WFs, and prefix Δ indicates the small variation of variable(s). Note that each wind farm is modelled as an aggregated PMSG-based wind turbine(PMSG-WT) connected with a transformer. Based on (1), the transfer function matrix of PMSG subsystem can be written as

$$\Delta I_{\mathrm{xy}}=H(s)\Delta V_{\mathrm{xy}}\tag{2}$$

where

$$\begin{aligned}\Delta I_{\mathrm{xy}}&=[\Delta I_{\mathrm{x1}}\quad \Delta I_{\mathrm{y1}}\quad \ldots\quad \Delta I_{\mathrm{x}p}\quad \Delta I_{\mathrm{y}p}]^{\mathrm{T}}\\ \Delta V_{\mathrm{xy}}&=[\Delta V_{\mathrm{x1}}\quad \Delta V_{\mathrm{y1}}\quad \ldots\quad \Delta V_{\mathrm{x}p}\quad \Delta V_{\mathrm{y}p}]^{\mathrm{T}}\\ H(s)&=C_{\mathrm{w}}(sI-A_{\mathrm{w}})^{-1}B_{\mathrm{w}}\end{aligned}\tag{3}$$

and I is the identity matrix of proper dimension. As for ROPS subsystem, its linearized state equation can be written as

$$\begin{cases} \dfrac{\mathrm{d}}{\mathrm{d}t}\Delta X_{\mathrm{G}} = A_{\mathrm{G}}\Delta X_{\mathrm{G}} + B_{\mathrm{G}}\Delta I_{\mathrm{xy}} \\ \Delta V_{\mathrm{xy}} = C_{\mathrm{G}}\Delta X_{\mathrm{G}} + D_{\mathrm{G}}\Delta I_{\mathrm{xy}} \end{cases} \tag{4}$$

where X_{G} is the vector of all the state variables of ROPS subsystem, and A_{G} is the state matrix of ROPS subsytem. And, the transfer function matrix of ROPS subsystem is

$$\Delta V_{\mathrm{xy}} = M(s)\Delta I_{\mathrm{xy}} \tag{5}$$

where

$$M(s) = C_{\mathrm{G}}(sI - A_{\mathrm{G}})^{-1}B_{\mathrm{G}} + D_{\mathrm{G}} \tag{6}$$

For calculation of the residue of open-loop modes of PMSG subsystem, the mutimachine power system should be regarded as the feedback connection of PMSG subsystem and ROPS subsystem, as shown in Fig. 2. However, in order to calculate the residue of open-loop modes of ROPS subsystem, virtual transfer functions $H'(s)$ and $M'(s)$ should be introduced, because $D_{\mathrm{G}} \neq \mathbf{O}$, according to the hybrid formulation for the sensitivity [13]. At the same time, the multimachine power system need to be treated as the feedback connection of a modified ROPS subsystem and a modified PMSG subsystem, as demonstrated in Fig. 3. $H'(s)$, $M'(s)$ in Fig. 3 are derived as follow

$$\begin{aligned} &H'(s) = C_{\mathrm{w}}(s\mathrm{I} - A_{\mathrm{w}})^{-1}B_{\mathrm{w}}[I - D_{\mathrm{G}}H(s)]^{-1} \\ &M'(s) = M(s) - D_{\mathrm{G}} \\ &\Delta V'_{\mathrm{xy}} = [I - D_{\mathrm{G}}H(s)]\Delta V_{\mathrm{xy}} \end{aligned} \tag{7}$$

Besides, the linearized closed-loop model of the entire power system can be expressed as

$$\frac{\mathrm{d}}{\mathrm{d}t}\Delta X = A\Delta X \tag{8}$$

where

$$\Delta X = [\Delta X_{\mathrm{G}}^{\mathrm{T}} \quad \Delta X_{\mathrm{w}}^{\mathrm{T}}]^{\mathrm{T}}$$

$$A = \begin{bmatrix} A_{\mathrm{w}} + B_{\mathrm{w}}D_{\mathrm{G}}C_{\mathrm{w}} & B_{\mathrm{w}}C_{\mathrm{G}} \\ B_{\mathrm{G}}C_{\mathrm{w}} & A_{\mathrm{G}} \end{bmatrix} \tag{9}$$

B. Formation of ALFMA and ALFMR

Under normal operating conditions, the dynamic interactions between PMSG subsystem and ROPS subsystem are weak such that PMSG subsystem and ROPS subsystem can be recognized as almost decoupled. This recognition has been explained in [4]. Therefore, within the range of the frequency of LFO, both ΔV_{xy} in Fig. 2 and $\Delta V'_{\mathrm{xy}}$ in Fig. 3 are usually very small, i.e., $\Delta V_{\mathrm{xy}} \approx 0$ and $\Delta V'_{\mathrm{xy}} \approx 0$. And, based on this recognition, a small positive number ξ, $0 < \xi << 1$, can be introduced and the transfer function matrix of the ROPS subsystem can be rewritten as $M(s) = \xi R(s)$, where

$$\begin{aligned} M(s) &= \xi R(s) = \frac{\xi r(s)}{s - \lambda_{\mathrm{g}i}} \\ H(s) &= \frac{h(s)}{s - \lambda_{\mathrm{wh},i}} \end{aligned} \tag{10}$$

$$\begin{aligned} \xi r(s) &= R_{\mathrm{g}i} + (s - \lambda_{\mathrm{g}i})\left(\sum_{j=1,j\neq i}^{n_{\mathrm{g}}} \frac{R_{\mathrm{g}j}}{s - \lambda_{\mathrm{g}j}} + D_{\mathrm{G}}\right) \\ h(s) &= R_{\mathrm{wh},i} + (s - \lambda_{\mathrm{wh},i})\left(\sum_{j=1,j\neq i}^{n_{\mathrm{wh}}} \frac{R_{\mathrm{wh},j}}{s - \lambda_{\mathrm{wh},j}}\right) \\ &\quad + (s - \lambda_{\mathrm{wh},i})\left(\sum_{l=1,l\neq h}^{p}\sum_{j=1}^{n_{\mathrm{wl}}} \frac{R_{\mathrm{wl},j}}{s - \lambda_{\mathrm{wl},j}}\right) \end{aligned} \tag{11}$$

$\lambda_{\mathrm{g}i}$ is the ith eigenvalue of A_G, $\lambda_{\mathrm{wh},i}(h = 1, ..., p, i = 1, ..., n_{\mathrm{wh}})$ is the ith eigenvalue of A_{wh}, n_{g} is the dimension of A_G, n_{wh} is the dimension of A_{wh}, $R_{\mathrm{g}i} = C_{\mathrm{G}}v_{\mathrm{g}i}w_{\mathrm{g}i}^T B_{\mathrm{G}}$, $R_{\mathrm{wh},i} = C_{\mathrm{w}}v_{\mathrm{wh},i}w_{\mathrm{wh},i}^T B_{\mathrm{w}}$, $v_{\mathrm{g}i}$ is the right eigenvector corresponding to $\lambda_{\mathrm{g}i}$, $w_{\mathrm{g}i}$ is the left eigenvector corresponding to $\lambda_{\mathrm{g}i}$, $v_{\mathrm{wh},i}$ is the right eigenvector of A_{w} corresponding to $\lambda_{\mathrm{wh},i}$, and $w_{\mathrm{wh},i}$ is the left eigenvector of A_{w} corresponding to $\lambda_{\mathrm{wh},i}$.

In most cases, all elements of A in (9) are continuously differentiable with respect to ξ. Also, $\lim_{\xi\to 0}\|D_{\mathrm{G}}\| = 0$, and either $\lim_{\xi\to 0}\|C_{\mathrm{G}}\| = 0$ or $\lim_{\xi\to 0}\|B_{\mathrm{G}}\| = 0$, where $\|P\|$ denotes the maximum singular value of matrix P. As a result, all eigenvalues of A are continuously differentiable with respect ξ [14]. Moreover, when $\xi = 0$, the eigenvalues of A are composed of eigenvalues of A_{G} and eigenvalues of A_{w}. To be more specific, for $\lambda_{\mathrm{g}i}$, also an eigenvalue of A when $\xi = 0$, it moves to $\hat{\lambda}_{\mathrm{g}i}$, as ξ becomes positive. And, $\Delta\lambda_{\mathrm{g}i}$, the difference between $\hat{\lambda}_{\mathrm{g}i}$ and $\lambda_{\mathrm{g}i}$, can be approximately expressed as(see proof in the Appendix)

$$\Delta\lambda_{\mathrm{g}i} \approx \xi\frac{\mathrm{tr}[h(\lambda_{\mathrm{g}i})r(\lambda_{\mathrm{g}i})]}{\lambda_{\mathrm{g}i} - \lambda_{\mathrm{wh},i}}, \tag{12}$$

where $\mathrm{tr}(A)$ denotes the trace of matrix A. Similarly, for $\lambda_{\mathrm{wh},i}$ and the corresponding $\hat{\lambda}_{\mathrm{wh},i}$, it can be derived that

$$\Delta\lambda_{\mathrm{wh},i} \approx \xi\frac{\mathrm{tr}[h(\lambda_{\mathrm{wh},i})r(\lambda_{\mathrm{wh},i})]}{\lambda_{\mathrm{wh},i} - \lambda_{\mathrm{g}i}} \tag{13}$$

When $\lambda_{\mathrm{g}i}$ is not close to $\lambda_{\mathrm{wh},i}$, equations (12) and (13) show that $\Delta\lambda_{\mathrm{g}i}$ and $\Delta\lambda_{\mathrm{wh},i}$ are small under the condition of $0 < \xi << 1$. However, as system parameters or operating condition change, $\lambda_{\mathrm{g}i}$ may become close to $\lambda_{\mathrm{wh},i}$, causing $\Delta\lambda_{\mathrm{g}i}$ and $\Delta\lambda_{\mathrm{wh},i}$ to become significant. Such phenomenon is called LFMR. And, $\lambda_{\mathrm{g}i}$ and $\lambda_{\mathrm{wh},i}$ are defined as the pair of open-loop LFO modes participating in the LFMR. $\hat{\lambda}_{\mathrm{g}i}$ and $\hat{\lambda}_{\mathrm{wh},i}$ are said to be the corresponding pair of closed-loop LFO modes. For a specified parameter set in parameter space, if the following

requirements on the pair of open-loop LFO modes can be met as system parameters vary within the set,

$$\begin{aligned}\lambda_{\mathrm{g}i} &= \lambda_{\mathrm{w}h,i}\\ \Delta\lambda_{\mathrm{g}i} &= \Delta\lambda_{\mathrm{w}h,i}\end{aligned} \tag{14}$$

then the LFMR occurred in the system is considered to be symmetric. Otherwise, the LFMR occurred in the system is regarded as asymmetric. As for asymmetric LFMR, within the parameter set, there is a group of parameters, under which $|\lambda_{\mathrm{g}i}-\lambda_{\mathrm{w}h,i}|$ reaches the minimum. That group of parameters correspond to a parameter vector in the parameter space, and the endpoint of the vector is defined as near open-loop modal resonance(NOLMR) point. Once the endpoint of the parameter vector of the system reaches the NOLMR point, if

$$\mathrm{Re}(\lambda_{\mathrm{w}h,i}) < \mathrm{Re}(\lambda_{\mathrm{g}i}), \quad \mathrm{Re}(\Delta\lambda_{\mathrm{g}i}) < 0$$

or

$$\mathrm{Re}(\lambda_{\mathrm{w}h,i}) > \mathrm{Re}(\lambda_{\mathrm{g}i}), \quad \mathrm{Re}(\Delta\lambda_{\mathrm{g}i}) > 0$$

then ALFMA happens in the system. On the other hand, if

$$\mathrm{Re}(\lambda_{\mathrm{w}h,i}) < \mathrm{Re}(\lambda_{\mathrm{g}i}), \quad \mathrm{Re}(\Delta\lambda_{\mathrm{g}i}) > 0$$

or

$$\mathrm{Re}(\lambda_{\mathrm{w}h,i}) > \mathrm{Re}(\lambda_{\mathrm{g}i}), \quad \mathrm{Re}(\Delta\lambda_{\mathrm{g}i}) < 0$$

then ALFMR occurs in the system. In comparison to symmetric LFMR, it is much easier for asymmetric LFMR to occur in power system.

C. Detection of ALFMA and ALFMR

In order to detect ALFMA and ALFMR, a residue based open-loop modal analysis method is proposed for estimating the trajectories of closed-loop LFO modes as system parameters vary. The method is derived as follows.

Assume that $\lambda_{\mathrm{g}i}$ and $\lambda_{\mathrm{w}h,i}$ are the identified pair of open-loop modes participating in the LFMR. Then, for $M(s)$ and $H(s)$ in Fig. 2, they can be expressed as

$$\begin{aligned}M(s) &= \frac{R_{\mathrm{g}i}}{s-\lambda_{\mathrm{g}i}} + \sum_{j=1,j\neq i}^{n_{\mathrm{g}}} \frac{R_{\mathrm{g}j}}{s-\lambda_{\mathrm{g}j}} + D_{\mathrm{G}}\\ H(s) &= \frac{R_{\mathrm{w}h,i}}{s-\lambda_{\mathrm{w}h,i}} + \sum_{j=1,j\neq i}^{n_{\mathrm{w}h}} \frac{R_{\mathrm{w}h,j}}{s-\lambda_{\mathrm{w}h,j}}\\ &\quad + \sum_{l=1,l\neq h}^{p}\sum_{j=1}^{n_{\mathrm{w}l}} \frac{R_{\mathrm{w}l,j}}{s-\lambda_{\mathrm{w}l,j}}\end{aligned} \tag{15}$$

Also, for $M'(s)$ and $H'(s)$ in Fig. 3, they can be written as

$$\begin{aligned}M'(s) &= \left(\frac{R_{\mathrm{g}i}}{s-\lambda_{\mathrm{g}i}} + \sum_{j=1,j\neq i}^{n_{\mathrm{g}}} \frac{R_{\mathrm{g}j}}{s-\lambda_{\mathrm{g}j}}\right)\\ H'(s) &= \left(\frac{R_{\mathrm{w}h,i}}{s-\lambda_{\mathrm{w}h,i}} + \sum_{j=1,j\neq i}^{n_{\mathrm{w}h}} \frac{R_{\mathrm{w}h,j}}{s-\lambda_{\mathrm{w}h,j}}\right.\\ &\quad \left. + \sum_{l=1,l\neq h}^{p}\sum_{j=1}^{n_{\mathrm{w}l}} \frac{R_{\mathrm{w}l,j}}{s-\lambda_{\mathrm{w}l,j}}\right)[I-D_{\mathrm{G}}H(s)]^{-1}\end{aligned} \tag{16}$$

According to Fig. 2 and Fig. 3, the characteristic equation of the entire power system can be written as

$$\mathrm{Det}[I-H(s)M(s)] = 0 \tag{17}$$

or

$$\mathrm{Det}[I-H'(s)M'(s)] = 0 \tag{18}$$

where $\mathrm{Det}(A)$ denotes the determinant of matrix A. Substituting (15) and (16) into (17) and (18), we have

$$\begin{aligned}&\mathrm{Det}\left(I-\left(\frac{R_{\mathrm{g}i}}{s-\lambda_{\mathrm{g}i}} + \sum_{j=1,j\neq i}^{n_{\mathrm{g}}} \frac{R_{\mathrm{g}j}}{s-\lambda_{\mathrm{g}j}}\right)\left(\frac{R_{\mathrm{w}h,i}}{s-\lambda_{\mathrm{w}h,i}}\right.\right.\\ &\quad + \sum_{j=1,j\neq i}^{n_{\mathrm{w}h}} \frac{R_{\mathrm{w}h,j}}{s-\lambda_{\mathrm{w}h,j}} + \sum_{l=1,l\neq h}^{p}\sum_{j=1}^{n_{\mathrm{w}l}} \frac{R_{\mathrm{w}l,j}}{s-\lambda_{\mathrm{w}l,j}}\Bigg)\\ &\quad \left.[I-D_{\mathrm{G}}H(s)]^{-1}\right) = 0\end{aligned} \tag{19}$$

and

$$\begin{aligned}&\mathrm{Det}\left(I-\left(\frac{R_{\mathrm{w}h,i}}{s-\lambda_{\mathrm{w}h,i}} + \sum_{j=1,j\neq i}^{n_{\mathrm{w}h}} \frac{R_{\mathrm{w}h,j}}{s-\lambda_{\mathrm{w}h,j}} + \sum_{l=1,l\neq h}^{p}\sum_{j=1}^{n_{\mathrm{w}l}}\right.\right.\\ &\quad \left.\left.\frac{R_{\mathrm{w}l,j}}{s-\lambda_{\mathrm{w}l,j}}\right)\left(\frac{R_{\mathrm{g}i}}{s-\lambda_{\mathrm{g}i}} + \sum_{j=1,j\neq i}^{n_{\mathrm{g}}} \frac{R_{\mathrm{g}j}}{s-\lambda_{\mathrm{g}j}} + D_{\mathrm{G}}\right)\right) = 0\end{aligned} \tag{20}$$

Multiplying both sides of (19) by $s-\lambda_{\mathrm{g}i}$

$$\begin{aligned}&\mathrm{Det}\left((s-\lambda_{\mathrm{g}i})I-\left(R_{\mathrm{g}i} + \sum_{j=1,j\neq i}^{n_{\mathrm{g}}} \frac{R_{\mathrm{g}j}(s-\lambda_{\mathrm{g}i})}{s-\lambda_{\mathrm{g}j}}\right)\right.\\ &\quad \left.\left(\sum_{l=1}^{p}\sum_{j=1}^{n_{\mathrm{w}l}} \frac{R_{\mathrm{w}l,j}}{s-\lambda_{\mathrm{w}l,j}}\right)[I-D_{\mathrm{G}}H(s)]^{-1}\right) = 0\end{aligned} \tag{21}$$

Similarly, via multiplying both side of (20) multiply by $s-\lambda_{\mathrm{w}h,i}$

$$\begin{aligned}&\mathrm{Det}\left((s-\lambda_{\mathrm{w}h,i})I-\left(R_{\mathrm{w}h,i} + \sum_{j=1,j\neq i}^{n_{\mathrm{w}h}} \frac{R_{\mathrm{w}h,j}(s-\lambda_{\mathrm{w}h,i})}{s-\lambda_{\mathrm{w}h,j}}\right.\right.\\ &\quad \left.\left. + \sum_{l=1,l\neq h}^{p}\sum_{j=1}^{n_{\mathrm{w}l}} \frac{R_{\mathrm{w}l,j}(s-\lambda_{\mathrm{w}h,i})}{s-\lambda_{\mathrm{w}l,j}}\right)\right.\\ &\quad \left.\left(\frac{R_{\mathrm{g}i}}{s-\lambda_{\mathrm{g}i}} + \sum_{j=1,j\neq i}^{n_{\mathrm{g}}} \frac{R_{\mathrm{g}j}}{s-\lambda_{\mathrm{g}j}} + D_{\mathrm{G}}\right)\right) = 0\end{aligned} \tag{22}$$

Replacing s with $\hat{\lambda}_{\mathrm{g}i}$ in (21), we can obtain that

$$\begin{aligned}&\mathrm{Det}\left((\hat{\lambda}_{\mathrm{g}i}-\lambda_{\mathrm{g}i})I-\left(R_{\mathrm{g}i} + \sum_{j=1,j\neq i}^{n_{\mathrm{g}}} \frac{R_{\mathrm{g}j}(\hat{\lambda}_{\mathrm{g}i}-\lambda_{\mathrm{g}i})}{\hat{\lambda}_{\mathrm{g}i}-\lambda_{\mathrm{g}j}}\right)\right.\\ &\quad \left.\left(\sum_{l=1}^{p}\sum_{j=1}^{n_{\mathrm{w}l}} \frac{R_{\mathrm{w}l,j}}{\hat{\lambda}_{\mathrm{g}i}-\lambda_{\mathrm{w}l,j}}\right)[I-D_{\mathrm{G}}H(\hat{\lambda}_{\mathrm{g}i})]^{-1}\right) = 0\end{aligned} \tag{23}$$

When $s=\hat{\lambda}_{\mathrm{w}hi}$ in (22)

$$\mathrm{Det}\Bigg((\hat{\lambda}_{\mathrm{w}h,i}-\lambda_{\mathrm{w}h,i})I-\Bigg(R_{\mathrm{w}h,i}+\sum_{j=1,j\neq i}^{n_{\mathrm{w}h}}\frac{R_{\mathrm{w}h,j}(\hat{\lambda}_{\mathrm{w}h,i}-\lambda_{\mathrm{w}h,i})}{\hat{\lambda}_{\mathrm{w}h,i}-\lambda_{\mathrm{w}h,j}}+\sum_{l=1,l\neq h}^{p}\sum_{j=1}^{n_{\mathrm{w}l}}\frac{R_{\mathrm{w}l,j}(\hat{\lambda}_{\mathrm{w}h,i}-\lambda_{\mathrm{w}h,i})}{\hat{\lambda}_{\mathrm{w}h,i}-\lambda_{\mathrm{w}l,j}}\Bigg)\Bigg(\frac{R_{\mathrm{g}i}}{\hat{\lambda}_{\mathrm{w}h,i}-\lambda_{\mathrm{g}i}}+\sum_{j=1,j\neq i}^{n_{\mathrm{g}}}\frac{R_{\mathrm{g}j}}{\hat{\lambda}_{\mathrm{w}h,i}-\lambda_{\mathrm{g}j}}+D_{\mathrm{G}}\Bigg)\Bigg)=0 \quad (24)$$

Once $|\hat{\lambda}_{\mathrm{g}i}-\lambda_{\mathrm{g}i}|$ is small, (23) is approximately equivalent to

$$\begin{aligned}&\mathrm{Det}((\hat{\lambda}_{\mathrm{g}i}-\lambda_{\mathrm{g}i})I-\Omega)=0\\&\Omega=R_{\mathrm{g}i}H'(\lambda_{\mathrm{g}i})\end{aligned} \quad (25)$$

At the same time, as long as $|\hat{\lambda}_{\mathrm{w}h,i}-\lambda_{\mathrm{w}h,i}|$ is small, (24) can be approximated by

$$\begin{aligned}&\mathrm{Det}((\hat{\lambda}_{\mathrm{w}h,i}-\lambda_{\mathrm{w}h,i})I-\Upsilon)=0\\&\Upsilon=R_{\mathrm{w}h,i}M(\lambda_{\mathrm{w}h,i})\end{aligned} \quad (26)$$

Because $v_{\mathrm{g}i}$ and $v_{\mathrm{w}h,i}$ are column vectors, and $w_{\mathrm{g}i}^{\mathrm{T}}$ and $w_{\mathrm{w}h,i}^{\mathrm{T}}$ are row vectors, $\mathrm{rank}(R_{\mathrm{g}i})\leq 1$ and $\mathrm{rank}(R_{\mathrm{w}h,i})\leq 1$. As a result, $\mathrm{rank}(\Omega)\leq 1$ and $\mathrm{rank}(\Upsilon)\leq 1$. So Ω and Υ have at most one nonzero eigenvalue respectively. Note that $\hat{\lambda}_{\mathrm{g}i}-\lambda_{\mathrm{g}i}$, the solution of (25), equals one of the eigenvalues of Ω. If $\mathrm{rank}(\Omega)=1$, the nonzero eigenvalue of Ω can be expressed as

$$\hat{\lambda}_{\mathrm{g}i}-\lambda_{\mathrm{g}i}=\mathrm{tr}(R_{\mathrm{g}i}H'(\lambda_{\mathrm{g}i}))=w_{\mathrm{g}i}^{\mathrm{T}}B_{\mathrm{G}}H'(\lambda_{\mathrm{g}i})C_{\mathrm{G}}v_{\mathrm{g}i} \quad (27)$$

Also, if $\mathrm{rank}(\Upsilon)=1$, then the nonzero eigenvalue of Υ is

$$\hat{\lambda}_{\mathrm{w}h,i}-\lambda_{\mathrm{w}h,i}=\mathrm{tr}(R_{\mathrm{w}h,i}M(\lambda_{\mathrm{w}h,i}))=w_{\mathrm{w}h,i}^{\mathrm{T}}B_{\mathrm{w}}M(\lambda_{\mathrm{w}h,i})C_{\mathrm{w}}v_{\mathrm{w}h,i} \quad (28)$$

Besides, if $\mathrm{rank}(\Omega)=0$, then $\mathrm{tr}(R_{\mathrm{g}i}H'(\lambda_{\mathrm{g}i}))=0$. Similarly, $\mathrm{tr}(R_{\mathrm{w}h,i}M(\lambda_{\mathrm{w}h,i}))=0$ when $\mathrm{rank}(\Upsilon)=0$.

Based on the above discussions, an estimate of $\hat{\lambda}_{\mathrm{g}i}$ and $\hat{\lambda}_{\mathrm{w}h,i}$ can be obtained as follow

$$\begin{aligned}&\tilde{\hat{\lambda}}_{\mathrm{g}i}=\lambda_{\mathrm{g}i}+w_{\mathrm{g}i}^{\mathrm{T}}B_{\mathrm{G}}H'(\lambda_{\mathrm{g}i})C_{\mathrm{G}}v_{\mathrm{g}i}\\&\tilde{\hat{\lambda}}_{\mathrm{w}h,i}=\lambda_{\mathrm{w}h,i}+w_{\mathrm{w}h,i}^{\mathrm{T}}B_{\mathrm{w}}M(\lambda_{\mathrm{w}h,i})C_{\mathrm{w}}v_{\mathrm{w}h,i}\end{aligned} \quad (29)$$

The estimation asserts that $\tilde{\hat{\lambda}}_{\mathrm{g}i}-\lambda_{\mathrm{g}i}$ is the nonzero eigenvalue of Ω if $\mathrm{rank}(\Omega)=1$. The accuracy of the estimation will be analyzed in the next subsection.

D. Analysis of Estimation Error of the Location of Closed-loop LFO Modes

In the first place, denote

$$\Gamma(\Delta\lambda_{\mathrm{g}i})=\left(R_{\mathrm{g}i}+\sum_{j=1,j\neq i}^{n_{\mathrm{g}}}\frac{R_{\mathrm{g}j}\Delta\lambda_{\mathrm{g}i}}{\Delta\lambda_{\mathrm{g}i}+\lambda_{\mathrm{g}i}-\lambda_{\mathrm{g}j}}\right)\left(\sum_{l=1}^{p}\sum_{j=1}^{n_{\mathrm{w}l}}\frac{R_{\mathrm{w}l,j}}{\Delta\lambda_{\mathrm{g}i}+\lambda_{\mathrm{g}i}-\lambda_{\mathrm{w}l,j}}\right)[I-D_{\mathrm{G}}H(\Delta\lambda_{\mathrm{g}i}+\lambda_{\mathrm{g}i})]^{-1} \quad (30)$$

Obviously, equation $\mathrm{Det}((s-\lambda_{\mathrm{g}i})I-\Gamma(\Delta\lambda_{\mathrm{g}i}))=0$ is equivalent to

$$\prod_{k=1}^{2p}(s-\lambda_{\mathrm{g}i}-\mathrm{eig}_k(\Gamma(\Delta\lambda_{\mathrm{g}i})))=0 \quad (31)$$

where $\mathrm{eig}_k(\Gamma)$ is the kth eigenvalue of Γ. And, via the expansion of left-hand side of (31), it can be obtained that

$$\begin{aligned}&(s-\lambda_{\mathrm{g}i})^{2p}-(s-\lambda_{\mathrm{g}i})^{2p-1}\mathrm{tr}(\Gamma(0))\\&-(s-\lambda_{\mathrm{g}i})^{2p-1}(\mathrm{eig}_1(\Gamma(\Delta\lambda_{\mathrm{g}i}))\\&-\mathrm{tr}(\Gamma(0)))+(s-\lambda_{\mathrm{g}i})^{2p-1}(-\mathrm{eig}_2(\Gamma(\Delta\lambda_{\mathrm{g}i})))+\cdots\\&+(s-\lambda_{\mathrm{g}i})^{2p-1}(-\mathrm{eig}_{2p}(\Gamma(\Delta\lambda_{\mathrm{g}i})))+(s-\lambda_{\mathrm{g}i})^{2p-2}\times\\&\sum_{\substack{\mu_k\in\{0,1\}\\k=1,2,\cdots,2p\\\mu_1+\ldots+\mu_{2p}=2}}\left(\prod_{k=1}^{2p}(-\mathrm{eig}_k(\Gamma(\Delta\lambda_{\mathrm{g}i})))^{\mu_k}\right)+\cdots\\&+\mathrm{Det}(\Delta\lambda_{\mathrm{g}i})=0\end{aligned} \quad (32)$$

Furthermore, denote

$$\begin{aligned}&\Psi(\Delta\lambda_{\mathrm{g}i})=-(s-\lambda_{\mathrm{g}i})^{2p-1}(\mathrm{eig}_1(\Gamma(\Delta\lambda_{\mathrm{g}i}))-\mathrm{tr}(\Gamma(0)))\\&+(s-\lambda_{\mathrm{g}i})^{2p-1}(-\mathrm{eig}_2(\Gamma(\Delta\lambda_{\mathrm{g}i})))+\cdots\\&+(s-\lambda_{\mathrm{g}i})^{2p-1}(-\mathrm{eig}_{2p}(\Gamma(\Delta\lambda_{\mathrm{g}i})))+(s-\lambda_{\mathrm{g}i})^{2p-2}\times\\&\sum_{\substack{\mu_k\in\{0,1\}\\k=1,2,\cdots,2p\\\mu_1+\ldots+\mu_{2p}=2}}\left(\prod_{k=1}^{2p}(-\mathrm{eig}_k(\Gamma(\Delta\lambda_{\mathrm{g}i})))^{\mu_k}\right)+\cdots\\&+\mathrm{Det}(\Delta\lambda_{\mathrm{g}i})\end{aligned} \quad (33)$$

Then, (32) can be transformed into

$$(s-\lambda_{\mathrm{g}i})^{2p}-(s-\lambda_{\mathrm{g}i})^{2p-1}\mathrm{tr}(\Gamma(0))+\Psi(\Delta\lambda_{\mathrm{g}i})=0 \quad (34)$$

As can be seen, the exact closed-loop LFO mode, $\hat{\lambda}_{\mathrm{g}i}$, is the solution of (31). However, its estimate, $\tilde{\hat{\lambda}}_{\mathrm{g}i}$ is the solution of $\prod_{k=1}^{2p}(s-\lambda_{\mathrm{g}i}-\mathrm{eig}_k(\Gamma(0)))=0$. For analyzing the difference between $\hat{\lambda}_{\mathrm{g}i}$ and $\tilde{\hat{\lambda}}_{\mathrm{g}i}$, denote $\Delta\lambda_{\mathrm{g}i}=\alpha+j\beta$ and $s=\nu+j\kappa$ in order to rewrite (34) as

$$\begin{aligned}F_1(\alpha,\beta,\nu,\kappa)=&\mathrm{Re}((s-\lambda_{\mathrm{g}i})^{2p}-(s-\lambda_{\mathrm{g}i})^{2p-1}\mathrm{tr}(\Gamma(0))\\&+\Psi(\Delta\lambda_{\mathrm{g}i}))\\F_2(\alpha,\beta,\nu,\kappa)=&\mathrm{Im}((s-\lambda_{\mathrm{g}i})^{2p}-(s-\lambda_{\mathrm{g}i})^{2p-1}\mathrm{tr}(\Gamma(0))\\&+\Psi(\Delta\lambda_{\mathrm{g}i}))\end{aligned} \quad (35)$$

Since $F_1+jF_2=\mathrm{Det}((\nu+j\kappa-\lambda_{\mathrm{g}i})I-\Gamma(\alpha+j\beta))$, when $|\Delta\lambda_{\mathrm{g}i}|$ is small, both F_1 and F_2 are continuously differentiable with respect to ν and κ. The partial derivatives of F_1 and F_2 with respect to ν and κ are presented as follows.

$$\begin{aligned}
\frac{\partial F_1(\alpha,\beta,\nu,\kappa)}{\partial\nu} =&\mathrm{Re}\Bigg(\frac{\partial}{\partial\nu}((s-\lambda_{\mathrm{g}i})^{2p}-(s-\lambda_{\mathrm{g}i})^{2p-1}\mathrm{tr}(\Gamma(0))\\
&+\Psi(\Delta\lambda_{\mathrm{g}i}))\Bigg)\\
\frac{\partial F_1(\alpha,\beta,\nu,\kappa)}{\partial\kappa} =&\mathrm{Re}\Bigg(\frac{\partial}{\partial\kappa}((s-\lambda_{\mathrm{g}i})^{2p}-(s-\lambda_{\mathrm{g}i})^{2p-1}\mathrm{tr}(\Gamma(0))\\
&+\Psi(\Delta\lambda_{\mathrm{g}i}))\Bigg)\\
\frac{\partial F_2(\alpha,\beta,\nu,\kappa)}{\partial\nu} =&\mathrm{Im}\Bigg(\frac{\partial}{\partial\nu}((s-\lambda_{\mathrm{g}i})^{2p}-(s-\lambda_{\mathrm{g}i})^{2p-1}\mathrm{tr}(\Gamma(0))\\
&+\Psi(\Delta\lambda_{\mathrm{g}i}))\Bigg)\\
\frac{\partial F_2(\alpha,\beta,\nu,\kappa)}{\partial\kappa} =&\mathrm{Im}\Bigg(\frac{\partial}{\partial\kappa}((s-\lambda_{\mathrm{g}i})^{2p}-(s-\lambda_{\mathrm{g}i})^{2p-1}\mathrm{tr}(\Gamma(0))\\
&+\Psi(\Delta\lambda_{\mathrm{g}i}))\Bigg)
\end{aligned}\tag{36}$$

Via some algebraic manlpulates, it can be proved that

$$\begin{aligned}
\left.\frac{\partial F_1(\alpha,\beta,\nu,\kappa)}{\partial\nu}\right|_{\substack{\alpha+j\beta=0\\ \nu+j\kappa=s_0}} &= \mathrm{Re}(2p(s_0-\lambda_{\mathrm{g}i})^{2p-1}-\\
&\quad(2p-1)(s_0-\lambda_{\mathrm{g}i})^{2p-2}\mathrm{tr}(\Gamma(0)))\\
\left.\frac{\partial F_2(\alpha,\beta,\nu,\kappa)}{\partial\nu}\right|_{\substack{\alpha+j\beta=0\\ \nu+j\kappa=s_0}} &= \mathrm{Im}(2p(s_0-\lambda_{\mathrm{g}i})^{2p-1}-\\
&\quad(2p-1)(s_0-\lambda_{\mathrm{g}i})^{2p-2}\mathrm{tr}(\Gamma(0)))\\
\left.\frac{\partial F_1(\alpha,\beta,\nu,\kappa)}{\partial\kappa}\right|_{\substack{\alpha+j\beta=0\\ \nu+j\kappa=s_0}} &= \mathrm{Re}(j2p(s_0-\lambda_{\mathrm{g}i})^{2p-1}-\\
&\quad j(2p-1)(s_0-\lambda_{\mathrm{g}i})^{2p-2}\mathrm{tr}(\Gamma(0)))\\
\left.\frac{\partial F_2(\alpha,\beta,\nu,\kappa)}{\partial\kappa}\right|_{\substack{\alpha+j\beta=0\\ \nu+j\kappa=s_0}} &= \mathrm{Im}(j2p(s_0-\lambda_{\mathrm{g}i})^{2p-1}-\\
&\quad j(2p-1)(s_0-\lambda_{\mathrm{g}i})^{2p-2}\mathrm{tr}(\Gamma(0)))
\end{aligned}\tag{37}$$

where $s_0=\tilde{\hat{\lambda}}_{\mathrm{g}i}$, and

$$\begin{aligned}
&\mathrm{Det}\begin{pmatrix}\dfrac{\partial F_1(\alpha,\beta,\nu,\kappa)}{\partial\nu} & \dfrac{\partial F_2(\alpha,\beta,\nu,\kappa)}{\partial\nu}\\ \dfrac{\partial F_1(\alpha,\beta,\nu,\kappa)}{\partial\kappa} & \dfrac{\partial F_2(\alpha,\beta,\nu,\kappa)}{\partial\kappa}\end{pmatrix}\Bigg|_{\substack{\alpha+j\beta=0\\ \nu+j\kappa=s_0}}\\
&\qquad=|\mathrm{tr}(\Gamma(0))^{2p-1}|^2
\end{aligned}\tag{38}$$

As long as $\mathrm{rank}(\Gamma(0))=\mathrm{rank}(\Omega)=1$, which is more likely to be encountered, the inverse function theorem [15] can be applied to show that

$$\exists\mathcal{N}\{(0,0)\},\quad \mathcal{N}\{(\mathrm{Re}(\tilde{\hat{\lambda}}_{\mathrm{g}i}),\mathrm{Im}(\tilde{\hat{\lambda}}_{\mathrm{g}i}))\}$$

and a continuous function $T:\mathcal{N}\{(0,0)\}\to\mathcal{N}\{(\mathrm{Re}(\tilde{\hat{\lambda}}_{\mathrm{g}i}),\mathrm{Im}(\tilde{\hat{\lambda}}_{\mathrm{g}i}))\}$ satisfying $F_1(\alpha,\beta,T(\alpha,\beta))=0$ and $F_2(\alpha,\beta,T(\alpha,\beta))=0$ for all $(\alpha,\beta)\in\mathcal{N}\{(0,0)\}$, where $\mathcal{N}\{(\alpha,\beta)\}$ is the small neighbourhood of point (α,β). Because of the continuity of T, we can conclude that when $|\Delta\lambda_{\mathrm{g}i}|=\sqrt{\alpha^2+\beta^2}$ is small, $(\mathrm{Re}(\hat{\lambda}_{\mathrm{g}i}),\mathrm{Im}(\hat{\lambda}_{\mathrm{g}i}))\in\mathcal{N}\{(\mathrm{Re}(\tilde{\hat{\lambda}}_{\mathrm{g}i}),\mathrm{Im}(\tilde{\hat{\lambda}}_{\mathrm{g}i}))\}$ so $|\hat{\lambda}_{\mathrm{g}i}-\tilde{\hat{\lambda}}_{\mathrm{g}i}|$ is small. Similar analysis can show that $|\hat{\lambda}_{\mathrm{w}h,i}-\tilde{\hat{\lambda}}_{\mathrm{w}h,i}|$ is small once $\Delta\lambda_{\mathrm{w}h,i}$ is small.

III. Case studies

In this section, two study cases are presented to demonstrate the mechanism of asymmetric LFMR and the features of the proposed method. One case study is performed in a modified three-machine power system to show the existence of ALFMA influenced by the variation of k_{dci}, where k_{dci} is the integral gain of the PI controller in DC-link voltage control loop. The other case study is carried out on the 4-machine 11-bus power system with PMSG-WF integrated to demonstrate the existence of ALFMR affected by the variation of k_{dcp} and k_{dci}, where k_{dcp} is the proportional gain of the PI controller in DC-link voltage control loop.

A. The Study Case on the Modified Three-machine Power System

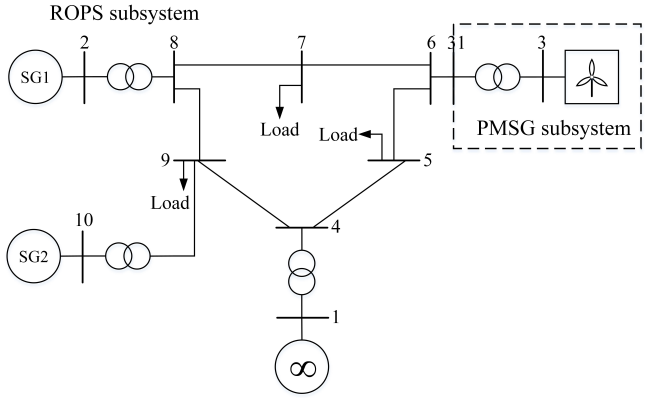

Fig. 4 Configuration of the three-machine power system

Fig. 4 shows the structure of the modified three-machine power system comprised of a PMSG-WF and two synchronous generators(SGs). The PMSG-WF is connected

at bus 31, while the 1st SG(SG1) is connected at bus 2 and the 2nd SG(SG2) is connected at bus 10. The wind farm consists of 70 PMSG-WTs. The detailed 13th-order model of the PMSG-WT, including its control systems, is given in [16]. Models and parameters of the two SGs, as well as transmission lines, transformers and loads are obtained from [14]. Note that bus 1 is an infinite bus.

As for ROPS subsystem, the eigenvalue of A_{G} corresponding to the open-loop power-angle mode(PAM) of SG is of great concern as it is sufficiently close to the imaginary axis on the complex plane, under a wide range of operating conditions and system parameters. To be worse, it is possible for the eigenvalue to interact with one or more eigenvalues of PMSG subsystem, causing ALFMR or ALFMA. If ALFMR happens, the small-signal stability of the entire power system may be lost. In this study case, the eigenvalue corresponding to the open-loop PAM of SG1, denoted as λ_{g1}, is $-0.1068 + j14.2821$, while the eigenvalue corresponding to the open-loop PAM of SG2, denoted as λ_{g2}, is $-0.0418+j6.3817$. Both λ_{g1} and λ_{g2} are forced to interact with the eigenvalue of A_{w} corresponding to the open-loop DC-link voltage mode(DCLVM) of the PMSG-WF, denoted as λ_{dc}, so as to study ALFMA.

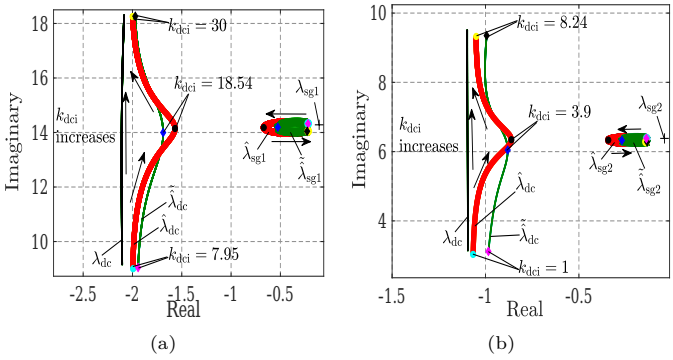

Fig. 5 Trajectories of eigenvalues and their estimates as k_{dci} increase from 1 to 30

In order to illustrate the existence of ALFMA originated from the interaction between λ_{g1}, λ_{g2} and λ_{dc}, k_{dci} is varied from $k_{\mathrm{dci}} = 1$ to $k_{\mathrm{dci}} = 30$. Note that the variation of k_{dci} exerts no influence on the operating condition of ROPS subsystem. Also, the proposed method is utilized to estimate the location of $\hat{\lambda}_{\mathrm{g1}}$,$\hat{\lambda}_{\mathrm{g2}}$ and $\hat{\lambda}_{\mathrm{dc}}$ for different values of k_{dci} ranging from 1 to 30. Note that $\hat{\lambda}_{\mathrm{g}i}(i = 1, 2)$ is the eigenvalue of A in (9) corresponding to the closed-loop PAM of SG$i(i = 1, 2)$, and $\hat{\lambda}_{\mathrm{dc}}$ is the eigenvalue of A corresponding to the closed-loop DCLVM of the PMSG-WF.

Table I: The actal and estimated locations of $\hat{\lambda}_{\mathrm{g1}}$ and $\hat{\lambda}_{\mathrm{dc}}$

	$k_{\mathrm{dci}} = 7.95$	$k_{\mathrm{dci}} = 18.54$	$k_{\mathrm{dci}} = 30$
$\hat{\lambda}_{\mathrm{g1}}$	-0.2179 + j14.325	-0.6688 + j14.1794	-0.2174+j14.0494
$\tilde{\hat{\lambda}}_{\mathrm{g1}}$	-0.2192+j14.3235	-0.5261+j14.1837	-0.2285+j14.0443
$\hat{\lambda}_{\mathrm{dc}}$	-1.9937+j9.0041	-1.5688+j14.1588	-1.9987+j18.2542
$\tilde{\hat{\lambda}}_{\mathrm{dc}}$	-1.943+j18.2542	-1.6884+j13.9987	-1.9714+j18.2658

Fig. 5(a) shows the location of λ_{g1} and the trajectories of $\hat{\lambda}_{\mathrm{g1}}$, λ_{dc} and $\hat{\lambda}_{\mathrm{dc}}$ as k_{dci} increases from 7.95 to 30. As is presented, $\mathrm{Re}(\lambda_{\mathrm{g1}}) > \mathrm{Re}(\lambda_{\mathrm{dc}})$ for all $k_{\mathrm{dci}} \in [7.95, 30]$. In addition, as k_{dci} increases from 7.95 to 18.54, the distance between λ_{dc} and λ_{g1} becomes smaller. But as k_{dci} increases further from 18.54 to 30, λ_{dc} begins to move away from λ_{g1}. When $k_{\mathrm{dci}} = 18.54$, $|\lambda_{\mathrm{g1}} - \lambda_{\mathrm{dc}}|$ reaches a local minimum. Moreover, as can be inferred from Table I, $\mathrm{Re}(\Delta\lambda_{\mathrm{g1}}) = -0.41925 < 0$ for $k_{\mathrm{dci}} = 18.54$. As a result, as k_{dci} varies between 7.95 and 30, ALFMA occurs in the modified three-machine system, resulted from the interaction between λ_{g1} and λ_{dc}. Besides, the estimates of $\hat{\lambda}_{\mathrm{g1}}$ and $\hat{\lambda}_{\mathrm{dc}}$ given by the proposed method, denoted as $\tilde{\hat{\lambda}}_{\mathrm{g1}}$ and $\tilde{\hat{\lambda}}_{\mathrm{dc}}$ respectively, are also demonstrated in Fig. 5(a). In particular, the values of $\hat{\lambda}_{\mathrm{g1}}$, $\hat{\lambda}_{\mathrm{dc}}$, $\tilde{\hat{\lambda}}_{\mathrm{g1}}$ and $\tilde{\hat{\lambda}}_{\mathrm{dc}}$ for $k_{\mathrm{dci}} = 7.95$, 18.54 and 30 are provided in Table I.

Table II: The actal and estimated locations of $\hat{\lambda}_{\mathrm{g2}}$ and $\hat{\lambda}_{\mathrm{dc}}$

	$k_{\mathrm{dci}} = 1$	$k_{\mathrm{dci}} = 3.9$	$k_{\mathrm{dci}} = 8.24$
$\hat{\lambda}_{\mathrm{g2}}$	-0.1370+j6.3811	-0.3426+j6.3338	-0.1409+j6.2808
$\tilde{\hat{\lambda}}_{\mathrm{g2}}$	-0.1386+j6.3781	-0.2695+j6.3236	-0.1347+j6.2810
$\hat{\lambda}_{\mathrm{dc}}$	-1.0661+j3.1161	-0.8615+j6.3433	-1.0497+j9.3265
$\tilde{\hat{\lambda}}_{\mathrm{dc}}$	-0.9844+j3.1187	-0.8811+j6.0456	-0.9939+j9.3496

Fig. 5(b) presents the location of λ_{g2} and the trajectories of $\hat{\lambda}_{\mathrm{g2}}$, λ_{dc} and $\hat{\lambda}_{\mathrm{dc}}$ as k_{dci} increases from 1 to 8.24. In Fig. 5(b), $\mathrm{Re}(\lambda_{\mathrm{g2}}) > \mathrm{Re}(\lambda_{\mathrm{dc}})$ for all $k_{\mathrm{dci}} \in [1, 8.24]$. Similar to Fig. 5(a), as k_{dci} increases from 1 to 3.9, λ_{dc} moves close to λ_{g2}. However, as k_{dci} increases further from 3.9 to 8.24, the difference between λ_{dc} and λ_{g2} becomes bigger. When $k_{\mathrm{dci}} = 3.9$, $|\lambda_{\mathrm{g2}} - \lambda_{\mathrm{dc}}|$ reaches a local minimum. Moreover, Table II indicates that $\mathrm{Re}(\Delta\lambda_{\mathrm{g2}}) = -0.2276851 < 0$ for $k_{\mathrm{dci}} = 3.9$. Therefore, as k_{dci} varies from 1 to 8.24, ALFMA occurs in the modified three-machine system, resulted from the interaction between λ_{g2} and λ_{dc}. In addition, the estimates of $\hat{\lambda}_{\mathrm{g2}}$ and $\hat{\lambda}_{\mathrm{dc}}$ provided by the proposed method, denoted as $\tilde{\hat{\lambda}}_{\mathrm{g2}}$ and $\tilde{\hat{\lambda}}_{\mathrm{dc}}$, are also shown in Fig. 5(b). Especially, the values of $\hat{\lambda}_{\mathrm{g2}}$, $\hat{\lambda}_{\mathrm{dc}}$, $\tilde{\hat{\lambda}}_{\mathrm{g2}}$ and $\tilde{\hat{\lambda}}_{\mathrm{dc}}$ for $k_{\mathrm{dci}} = 1$, 3.9 and 8.24 are provided in Table II. As can be seen from Fig. 5 ,Table I and Table II, the accuracy of estimation of the locations of $\hat{\lambda}_{dc}$, $\hat{\lambda}_{\mathrm{sg1}}$ and $\hat{\lambda}_{\mathrm{sg2}}$ provided by the proposed method is higher.

To confirm the existence of ALFMA from different aspects, time domain simulation is carried out on the three-machine power system. In the simulation, during the interval between 0.2s and 0.3s, the load at bus 6 is reduced to 90% of its initial value. Simulation results are presented in Fig. 6. According to Fig. 6(a) and (b), the oscillation of the power angle of SG1(δ_{SG1}) and DC-link voltage of the PMSG-WF(U_{dc}) decays faster as k_{dci} increases from 7.95 to 18.54. Moreover, the decay time constant and frequency of the oscillation of δ_{SG1} and U_{dc} are matched with those indicated by the real and imaginary part of $\hat{\lambda}_{\mathrm{g1}}$ and $\hat{\lambda}_{\mathrm{dc}}$ for $k_{\mathrm{dci}} = 7.95$ and 18.54. Similarly, as can be inferred from Fig. 6(c) and (d), the decay time constant and frequency of the oscillation of δ_{SG2} and U_{dc} are matched with those indicated by the real and imaginary part of $\hat{\lambda}_{\mathrm{g2}}$ and $\hat{\lambda}_{\mathrm{dc}}$ for $k_{\mathrm{dci}} = 1$ and 3.9.

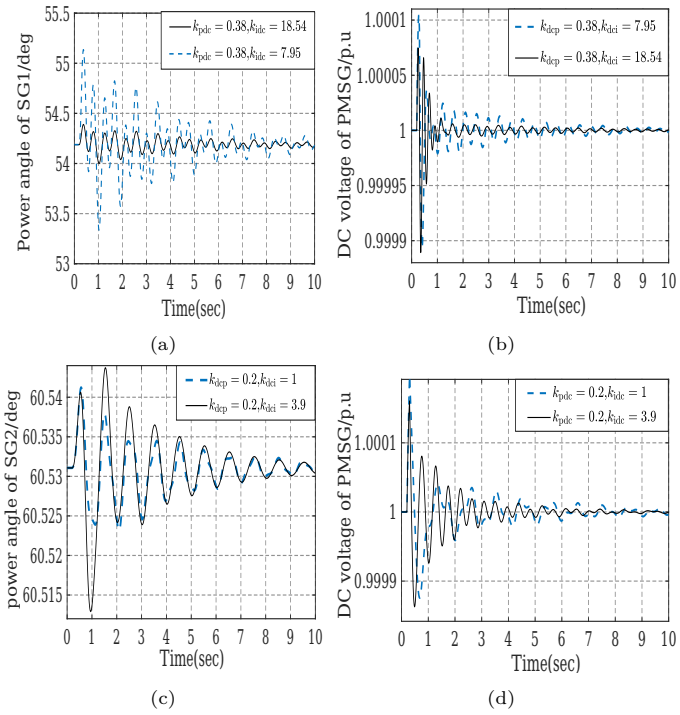

Fig. 6 Results of time domain simulation on the three-machine power system

B. The Study case on the 4-machine 11-bus Power System

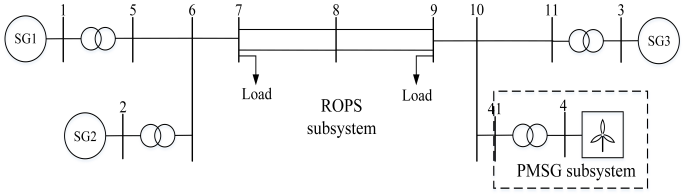

Fig. 7 Configuration of the 4-machine 11-bus power system

Fig.7 shows the configuration of 4-machine 11-bus power system comprised of a PMSG-WF and three SGs. The PMSG-WF is connected at bus 41, while the 1st SG(SG1), 2nd SG(SG2) and 3rd SG(SG3) are connected at bus 1, bus 2 and bus 3 respectively. There are 70 PMSG-WTs in the PMSG-WF. The model and parameters of the PMSG-WF are given in [16]. Models and parameters of transmission lines, transformers and loads are obtained from [14]. Models and parameters of the three SGs are given in [17].

As for ROPS subsystem, the eigenvalue of A_{G} corresponding to the open-loop speed mode(SM) of SG is also of great concern for its imaginary part is small, under a wide range of operating conditions and system parameters. Moreover, it is possible for the SM of ROPS subsystem to interact with one or more modes of PMSG subsystem, causing LFMR. In this case, the eigenvalue corresponding to the open-loop SM of SG2, denoted as λ_{r2}, is $-0.6592 + j18.0267$, and the eigenvalue corresponding to the open-loop SM of SG3, denoted as λ_{r3}, is $-0.3257 + j9.1205$. Both λ_{r2} and λ_{r3} tend to interact with the eigenvalue of A_{w} corresponding to the open-loop DCLVM of the PMSG-WF, so as to study ALFMR.

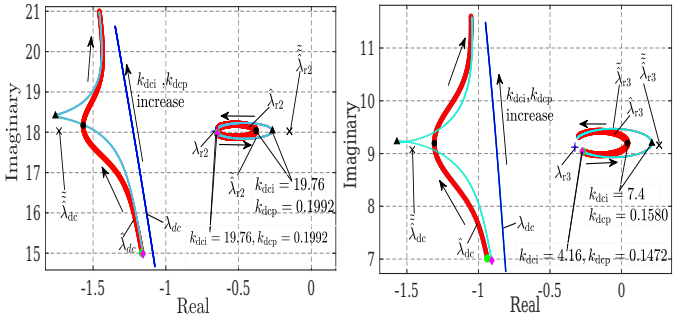

Fig. 8 Trajectories of eigenvalues and their estimates as k_{dcp} and k_{dci} increase from $k_{\mathrm{dcp}} = 0.1472$, $k_{\mathrm{dci}} = 4.16$ to $k_{\mathrm{dcp}} = 0.2621$, $k_{\mathrm{dci}} = 38.63$

In order to demonstrate the existence of ALFMR resulted from the interaction between λ_{r2}, λ_{r3} and λ_{dc}, k_{dcp} and k_{dci} are varied from $k_{\mathrm{dcp}} = 0.1472, k_{\mathrm{dci}} = 4.16$ to $k_{\mathrm{dcp}} = 0.2621, k_{\mathrm{dci}} = 38.63$. It is worth noting that the variation of k_{dcp} and k_{dci} brings no impact on the operating condition of ROPS subsystem. In addition, the locations of $\hat{\lambda}_{\mathrm{r2}}$, $\hat{\lambda}_{\mathrm{r3}}$ and $\hat{\lambda}_{\mathrm{dc}}$ are estimated by the proposed method with k_{dcp} and k_{dci} increasing from $k_{\mathrm{dcp}} = 0.1472, k_{\mathrm{dci}} = 4.16$ to $k_{\mathrm{dcp}} = 0.2621, k_{\mathrm{dci}} = 38.63$. Note that $\hat{\lambda}_{\mathrm{r}i}(i = 2, 3)$ is the eigenvalue of the state matrix of the entire power system, corresponding to the closed-loop SM of SG$i(i = 2, 3)$.

Fig. 8(a) displays the trajectories of λ_{r2}, $\hat{\lambda}_{\mathrm{r2}}$, λ_{dc} and $\hat{\lambda}_{\mathrm{dc}}$ as k_{dcp} and k_{dci} are tunned from $k_{\mathrm{dcp}} = 0.1992, k_{\mathrm{dci}} = 19.76$ to $k_{\mathrm{dcp}} = 0.2621, k_{\mathrm{dci}} = 38.63$. the figure indicates that $\mathrm{Re}(\lambda_{\mathrm{r2}}) > \mathrm{Re}(\lambda_{\mathrm{dc}})$ for all $k_{\mathrm{dcp}} \in [0.1992, 0.2621]$ and $k_{\mathrm{dci}} \in [19.76, 38.63]$. In addition, with k_{dci} increasing from 19.76 to 28.55 and k_{dcp} increasing from 0.1992 to 0.2285, the distance between λ_{dc} and λ_{r2} becomes smaller. But as k_{dcp} and k_{dci} increases further from $k_{\mathrm{dcp}} = 0.2285, k_{\mathrm{dci}} = 28.55$ to $k_{\mathrm{dcp}} = 0.2621, k_{\mathrm{dci}} = 38.63$, the distance between λ_{dc} and λ_{r2} becomes bigger. $|\lambda_{\mathrm{r2}} - \lambda_{\mathrm{dc}}|$ arrives at a local minimum when $k_{\mathrm{dcp}} = 0.2285, k_{\mathrm{dci}} = 28.55$. Furthermore, Table III indicates that $\mathrm{Re}(\Delta\lambda_{\mathrm{r2}}) = 0.2784 > 0$ when $k_{\mathrm{dcp}} = 0.2285, k_{\mathrm{dci}} = 28.55$. Therefore, ALFMR happens in the 4-machine 11-bus power system as k_{dcp} and k_{dci} vary from $k_{\mathrm{dcp}} = 0.1992, k_{\mathrm{dci}} = 19.76$ to $k_{\mathrm{dcp}} = 0.2621, k_{\mathrm{dci}} = 38.63$, due to the interaction between λ_{r2} and λ_{dc}. Besides, the estimates of $\hat{\lambda}_{\mathrm{dc}}$ and $\hat{\lambda}_{\mathrm{r2}}$ given by the proposed method, denoted as $\tilde{\hat{\lambda}}_{\mathrm{r2}}$ and $\tilde{\hat{\lambda}}_{\mathrm{dc}}$ respectively, as well as the estimates of $\hat{\lambda}_{\mathrm{dc}}$ and $\hat{\lambda}_{\mathrm{r2}}$ given by the method proposed in [11], denoted as $\tilde{\tilde{\hat{\lambda}}}_{\mathrm{r2}}$ and $\tilde{\tilde{\hat{\lambda}}}_{\mathrm{dc}}$ only for $k_{\mathrm{dcp}} = 0.2285, k_{\mathrm{dci}} = 28.55$, are demonstrated in Fig. 8(a). In particular, the values of $\tilde{\hat{\lambda}}_{\mathrm{r2}}$, $\tilde{\hat{\lambda}}_{\mathrm{dc}}$, $\tilde{\tilde{\hat{\lambda}}}_{\mathrm{r2}}$ and $\tilde{\tilde{\hat{\lambda}}}_{\mathrm{dc}}$ for $k_{\mathrm{dcp}} = 0.1992, k_{\mathrm{dci}} = 19.76$, $k_{\mathrm{dcp}} = 0.2285, k_{\mathrm{dci}} = 28.55$ and $k_{\mathrm{dcp}} = 0.2621, k_{\mathrm{dci}} = 38.63$ are listed in Table III.

Table III: The actal and estimated locations of $\hat{\lambda}_{r2}$ and $\hat{\lambda}_{dc}$

	$k_{dcp}=0.1992$ $k_{dci}=19.76$	$k_{dcp}=0.2285$ $k_{dci}=28.55$	$k_{dcp}=0.2621$ $k_{dci}=38.63$
$\hat{\lambda}_{r2}$	-0.6467+j17.9698	-0.3808+j18.0416	-0.6326+j18.1301
$\tilde{\hat{\lambda}}_{r2}$	-0.6466+j17.9695	-0.2673+j18.0358	-0.6366+j18.1233
$\tilde{\tilde{\hat{\lambda}}}_{r2}$	\	-0.1504+j18.0253	\
$\hat{\lambda}_{dc}$	-1.1637+j15.0058	-1.5679+j18.1729	-1.4568+j20.9997
$\tilde{\hat{\lambda}}_{dc}$	-1.1570+j14.9839	-1.7586+j18.4065	-1.4574+20.9770
$\tilde{\tilde{\hat{\lambda}}}_{dc}$	\	-1.7333+18.0311	\

Fig. 8(b) demonstrates the trajectaries of $\hat{\lambda}_{r3}$, λ_{dc} and $\hat{\lambda}_{dc}$, as well as the location of λ_{r3} with both k_{dcp} and k_{dci} increase from $k_{dcp}=0.1472$, $k_{dci}=4.16$ to $k_{dcp}=0.1739$, $k_{dci}=12.17$ respectively. As is presented, $\mathrm{Re}(\lambda_{r3})>\mathrm{Re}(\lambda_{dc})$ for all $k_{dcp}\in[0.1472,0.1739]$ and all $k_{dci}\in[4.16,12.17]$. In addition, the trend of $|\lambda_{r3}-\lambda_{dc}|$, as k_{dcp} and k_{dci} increase from $k_{dcp}=0.1472$,$k_{dci}=4.16$ to $k_{dcp}=0.1739$,$k_{dci}=12.17$, is similar to that of $|\lambda_{r2}-\lambda_{dc}|$ with k_{dcp} and k_{dci} tunned from $k_{dcp}=0.1992$, $k_{dci}=19.76$ to $k_{dcp}=0.2621$, $k_{dci}=38.63$. When $k_{dcp}=0.1580, k_{dci}=7.4$, $|\lambda_{r3}-\lambda_{dc}|$ reaches a local minimum. Moreover, as can be deduced from Table IV, $\mathrm{Re}(\Delta\lambda_{r3})=0.3672>0$ for $k_{dcp}=0.1580, k_{dci}=7.4$. Wherefore as k_{dcp} and k_{dci} tuning from 0.1472 ,4.16 to 0.1739,12.17, ALFMR arises in the 4-machine 11-bus power system, resulted from the interaction between λ_{r3} and λ_{dc}. Besides, the estimates of $\hat{\lambda}_{r3}$ and $\hat{\lambda}_{dc}$ given by the proposed method, denoted as $\tilde{\hat{\lambda}}_{r3}$ and $\tilde{\hat{\lambda}}_{dc}$ respectively, and the estimates of $\hat{\lambda}_{r3}$ and $\hat{\lambda}_{dc}$ given by the method proposed in [11], denoted as $\tilde{\tilde{\hat{\lambda}}}_{r3}$ and $\tilde{\tilde{\hat{\lambda}}}_{dc}$ respectively, are also displayed in Fig. 8(b). In particular, the values of $\tilde{\hat{\lambda}}_{r3}$, $\tilde{\hat{\lambda}}_{dc}$, $\tilde{\tilde{\hat{\lambda}}}_{r3}$ and $\tilde{\tilde{\hat{\lambda}}}_{dc}$ for $k_{dcp}=0.1472, k_{dci}=4.16$, $k_{dcp}=0.1580, k_{dci}=7.4$ and $k_{dcp}=0.1739, k_{dci}=12.17$ are listed in Table IV. It can be confirmed from Fig. 8, Table III and Table IV that compared to $\tilde{\tilde{\hat{\lambda}}}_{ri}$, $\tilde{\hat{\lambda}}_{ri}$ is closer to $\hat{\lambda}_{ri}$.

Table IV: The actal and estimated locations of $\hat{\lambda}_{r3}$ and $\hat{\lambda}_{dc}$

	$k_{dcp}=0.1472$ $k_{dci}=4.16$	$k_{dcp}=0.1580$ $k_{dci}=7.4$	$k_{dcp}=0.1739$ $k_{dci}=12.17$
$\hat{\lambda}_{r3}$	-0.2702+j9.0363	0.0415+j9.1970	-0.2974+j9.3309
$\tilde{\hat{\lambda}}_{r3}$	-0.2743+j9.0386	0.2120+j9.1953	-0.3071+j9.3015
$\tilde{\tilde{\hat{\lambda}}}_{r3}$	\	0.2631+j9.1585	\
$\hat{\lambda}_{dc}$	-0.9378+j7.0096	-1.3086+9.1954	-1.0516+j11.5989
$\tilde{\hat{\lambda}}_{dc}$	-0.9063+j6.9709	-1.5699+9.2224	-1.0454+11.5768
$\tilde{\tilde{\hat{\lambda}}}_{dc}$	\	-1.4622+9.074	\

To confirm the existence of ALFMR in different ways, time domain simulation is carried out on the 4-machine 11-bus power system. Simulation results are shown in Fig. 9. According to Fig. 9(a) and (b), the decay time constant and frequency of oscillation of the speed of SG2 and U_{dc} are matched with those indicated by the real and imaginary part of $\hat{\lambda}_{r2}$ and $\hat{\lambda}_{dc}$ for $k_{dcp}=0.1992$, $k_{dcp}=19.76$ and $k_{dcp}=0.2285$, $k_{dcp}=28.55$. Similarly, Fig. 9(c) and (d) reflect that the decay time constant and frequency of oscillation of the speed of SG3 and U_{dc} are matched with those indicated by the real and imaginary part of $\hat{\lambda}_{g3}$ and $\hat{\lambda}_{dc}$ for $k_{dcp}=0.1472$, $k_{dcp}=4,16$ and $k_{dcp}=0.1580$, $k_{dcp}=7.4$. What's worse, the small-signal stability of the entire power system is lost when $k_{dcp}=0.1580$, $k_{dcp}=7.4$.

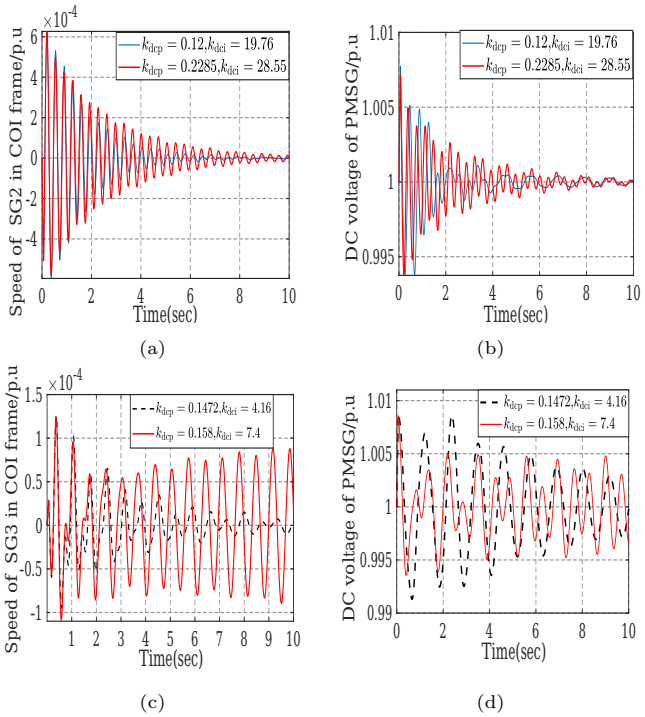

Fig. 9 Results of time domain simulation on the 4-machine 11-bus power system

IV. CONCLUSIONS

This paper has analyzed the mechanism of ALFMA and ALFMR in PMSG-WFs integrated power system. And, a residue based open-loop modal analysis method has been proposed for detecting ALFMA and ALFMR. As has been discussed, ALFMA and ALFMR are caused by the interaction between open-loop LFO modes of PMSG subsystem and ROPS subsystem as system parameters or operating conditions change. When ALFMR is encountered, the small-signal stability of the entire power system may be lost. On the other hand, if ALFMA occurs, the small-signal stability of the entire power system can be improved. According to the proposed method, both ALFMA and ALFMR are detected via estimating the trajectories of selected closed-loop LFO modes based on the residue of identified open-loop LFO modes. Simulation studies have confirmed that the estimates of the location of closed-loop LFO modes provided by the proposed method have higher accuracy than those given by the method proposed in [11].

The proposed method can be used for tunning the parameters of the controllers of PMSG-WF in order to prevent ALFMR from being excited in the entire power system. Besides, since the proposed method does not rely on the information of the eigenvalues of the state matrix of the entire power system, it may takes a shorter time

for the proposed method to perform small-signal stability analysis when the power system is complex.

Appendix

Derivation of formula (12) and (13):

Since $M(s)=\xi R(s)$, the characteristic equation of the entire power system shown in Fig.1 can be written as

$$\mathrm{Det}[I-H(s)\xi R(s)]=0 \tag{A1}$$

Substituting (11) into (A1), we have

$$\mathrm{Det}[\frac{(s-\lambda_{\mathrm{g}i})(s-\lambda_{\mathrm{wh},i})}{\xi}I-h(s)r(s)]=0 \tag{A2}$$

(A2) can be rewritten as

$$\begin{aligned}&[\frac{(s-\lambda_{\mathrm{g}i})(s-\lambda_{\mathrm{wh},i})}{\xi}]^{2p}+\\&a_{2p-1}(s)[\frac{(s-\lambda_{\mathrm{g}i})(s-\lambda_{\mathrm{wh},i})}{\xi}]^{2p-1}+\cdots+\\&a_1(s)\frac{(s-\lambda_{\mathrm{g}i})(s-\lambda_{\mathrm{wh},i})}{\xi}+a_0(s)=0\end{aligned} \tag{A3}$$

where $a_{2p-1}(s),\cdots,a_1(s),a_0(s)$ are all polynomials in s. Multiplying both sides of (A3) by $\frac{\xi^{2p}}{[(s-\lambda_{\mathrm{g}i})(s-\lambda_{\mathrm{wh},i})]^{2p-1}}$

$$\begin{aligned}&(s-\lambda_{\mathrm{g}i})(s-\lambda_{\mathrm{wh},i})+a_{2p-1}(s)\xi+\frac{a_{2p-2}(s)}{(s-\lambda_{\mathrm{g}i})(s-\lambda_{\mathrm{wh},i})}\xi^2\\&+\cdots+\frac{a_1(s)\xi^{2p-1}}{[(s-\lambda_{\mathrm{g}i})(s-\lambda_{\mathrm{wh},i})]^{2p-2}}\\&+\frac{a_0(s)\xi^{2p}}{[(s-\lambda_{\mathrm{g}i})(s-\lambda_{\mathrm{wh},i})]^{2p-1}}=0\end{aligned} \tag{A4}$$

Denote

$$\begin{aligned}&f_0(s)=(s-\lambda_{\mathrm{g}i})(s-\lambda_{\mathrm{wh},i}),f_1(s)=a_{2p-1}(s)\\&f_2(s)=\frac{a_{2p-2}(s)}{(s-\lambda_{\mathrm{g}i})(s-\lambda_{\mathrm{wh},i})}+\cdots+\\&\frac{a_1(s)\xi^{2p-3}}{[(s-\lambda_{\mathrm{g}i})(s-\lambda_{\mathrm{wh},i})]^{2p-2}}+\frac{a_0(s)\xi^{2p-2}}{[(s-\lambda_{\mathrm{g}i})(s-\lambda_{\mathrm{wh},i})]^{2p-1}}\end{aligned} \tag{A5}$$

With (A5), equation (A4) becomes

$$f_0(s)+\xi f_1(s)+\xi^2 f_2(s)=0 \tag{A6}$$

Since $\hat{\lambda}_{\mathrm{g}i}=\lambda_{\mathrm{g}i}+\Delta\lambda_{\mathrm{g}i}$, an eigenvalue of A(see (9)), is a solution of (A6),

$$f_0(\lambda_{\mathrm{g}i}+\Delta\lambda_{\mathrm{g}i})+\xi f_1(\lambda_{\mathrm{g}i}+\Delta\lambda_{\mathrm{g}i})+\xi^2 f_2(\lambda_{\mathrm{g}i}+\Delta\lambda_{\mathrm{g}i})=0 \tag{A7}$$

Replacing f_0, f_1 and f_2 with their Taylor series expansion at $\lambda_{\mathrm{g}i}$ is

$$\begin{aligned}&f_0(\lambda_{\mathrm{g}i})+f_0'(\lambda_{\mathrm{g}i})\Delta\lambda_{\mathrm{g}i}+\frac{f_0''(\lambda_{\mathrm{g}i})}{2!}\Delta\lambda_{\mathrm{g}i}^2+\cdots+\\&\xi[f_1(\lambda_{\mathrm{g}i})+f_1'(\lambda_{\mathrm{g}i})\Delta\lambda_{\mathrm{g}i}+\frac{f_1''(\lambda_{\mathrm{g}i})}{2!}\Delta\lambda_{\mathrm{g}i}^2+\cdots]\\&+\xi^2[f_2(\lambda_{\mathrm{g}i})+f_2'(\lambda_{\mathrm{g}i})\Delta\lambda_{\mathrm{g}i}+\frac{f_2''(\lambda_{\mathrm{g}i})}{2!}\Delta\lambda_{\mathrm{g}i}^2+\cdots]=0\end{aligned} \tag{A8}$$

According to [2] $\Delta\lambda_{\mathrm{g}i}$ can also be expressed as

$$\Delta\lambda_{\mathrm{g}i}=\beta_1\xi+\beta_2\xi^2+\beta_3\xi^3+\cdots \tag{A9}$$

where $\beta_k(k=1,2,3,\cdots)$ is complex coefficient to be determined. Substitute (A9) into (A8),

$$\begin{aligned}&f_0(\lambda_{\mathrm{g}i})+f_0'(\lambda_{\mathrm{g}i})(\beta_1\xi+\beta_2\xi^2+\beta_3\xi^3+\cdots+)\\&\frac{f_0''(\lambda_{\mathrm{g}i})}{2!}(\beta_1\xi+\beta_2\xi^2+\beta_3\xi^3+\cdots)^2+\cdots+\\&\xi[f_1(\lambda_{\mathrm{g}i})+f_1'(\lambda_{\mathrm{g}i})(\beta_1\xi+\beta_2\xi^2+\beta_3\xi^3+\cdots)+\\&\frac{f_1''(\lambda_{\mathrm{g}i})}{2!}(\beta_1\xi+\beta_2\xi^2+\beta_3\xi^3+\cdots)^2+\cdots]\\&+\xi^2[f_2(\lambda_{\mathrm{g}i})+f_2'(\lambda_{\mathrm{g}i})(\beta_1\xi+\beta_2\xi^2+\beta_3\xi^3+\cdots)+\\&\frac{f_2''(\lambda_{\mathrm{g}i})}{2!}(\beta_1\xi+\beta_2\xi^2+\beta_3\xi^3+\cdots)^2+\cdots]=0\end{aligned} \tag{A10}$$

Both sides of (A10) are polynomial of ξ. By equating the coefficients of the first-order term of ξ on the both sides of (A10), it can have that

$$\beta_1=\frac{-f_1(\lambda_{\mathrm{g}i})}{f_0'(\lambda_{\mathrm{g}i})} \tag{A11}$$

From (A5)

$$\begin{aligned}&f_0'(s)|_{s=\lambda_{\mathrm{g}i}}=(\lambda_{\mathrm{g}i}-\lambda_{\mathrm{wh}i})\\&f_1(\lambda_{\mathrm{g}i})=a_{2p-1}(\lambda_{\mathrm{g}i})=-\mathrm{tr}[h(\lambda_{\mathrm{g}i})r(\lambda_{\mathrm{g}i})]\end{aligned} \tag{A12}$$

Hence, the first-order approximation of $\Delta\lambda_{\mathrm{g}i}$, for $0<\xi\ll 1$, is obtained as

$$\Delta\lambda_{\mathrm{g}i}\approx\xi\frac{\mathrm{tr}[h(\lambda_{\mathrm{g}i})r(\lambda_{\mathrm{g}i})]}{\lambda_{\mathrm{g}i}-\lambda_{\mathrm{wh}i}} \tag{A13}$$

Besides, $\hat{\lambda}_{\mathrm{wh},i}=\lambda_{\mathrm{wh},i}+\Delta\lambda_{\mathrm{wh},i}$, another eigenvalue of A, is also a solution of (A6). Hence, taking the derivation similar to that from (A2) to (A13), it can have that

$$\Delta\lambda_{\mathrm{wh},i}\approx\xi\frac{\mathrm{tr}[h(\lambda_{\mathrm{wh},i})r(\lambda_{\mathrm{wh},i})]}{\lambda_{\mathrm{wh},i}-\lambda_{\mathrm{g}i}} \tag{A14}$$

References

[1] J. T. Bi, W. Du, and H. F. Wang, "Aggregated dynamic model of grid-connected pv generation farms," in International Conference on Renewable Power Generation (RPG 2015), 2015, pp. 1–6.

[2] M. I. Vishik and L. A. Lyusternik, "The solution of some perturbation problems for matrices and selfadjoint or non-selfadjoint differential equations i," RuMaS, vol. 15, no. 3, pp. 1–73, 1960.

[3] I. Dobson, J. Zhang, S. Greene, H. Engdahl, and P. W. Sauer, "Is strong modal resonance a precursor to power system oscillations?" IEEE Transactions on Circuits and Systems I: Fundamental Theory and Applications, vol. 48, no. 3, pp. 340–349, 2001.

[4] W. Du, X. Chen, and H. F. Wang, "Power system electromechanical oscillation modes as affected by dynamic interactions from grid-connected pmsgs for wind power generation," IEEE Transactions on Sustainable Energy, vol. 8, no. 3, pp. 1301–1312, 2017.

[5] M. Laughton, "Matrix analysis of dynamic stability in synchronous multimachine systems," in Proceedings of the Institution of Electrical Engineers, vol. 113, no. 2. IET, 1966, pp. 325–336.

[6] J. M. Uudrill, "Dynamic stability calculations for an arbitrary number of interconnected synchronous machines," IEEE Transactions on Power Apparatus and Systems, no. 3, pp. 835–844, 1968.

[7] R. Byerly, D. Sherman, and D. McLain, "Normal modes and mode shapes applied to dynamic stability analysis," IEEE Transactions on Power Apparatus and Systems, vol. 94, no. 2, pp. 224–229, 1975.
[8] F. D. Mello, P. Nolan, T. Laskowski, and J. Undrill, "Coordinated application of stabilizers in multimachine power systems," IEEE Transactions on Power Apparatus and Systems, vol. PAS-99, no. 3, pp. 892–901, 1980.
[9] F. P. Demello and C. Concordia, "Concepts of synchronous machine stability as affected by excitation control," IEEE Transactions on Power Apparatus and Systems, vol. PAS-88, no. 4, pp. 316–329, 1969.
[10] H. Gooi, E. Hill, M. Mobarak, D. Thorne, and T. Lee, "Coordinated multi-machine stabilizer settings without eigenvalue drift," IEEE Transactions on Power Apparatus and Systems, vol. PAS-100, no. 8, pp. 3879–3887, 1981.
[11] W. Du, Q. Fu, H. Wang, and Y. Wang, "Concept of modal repulsion for examining the subsynchronous oscillations caused by wind farms in power systems," IEEE Transactions on Power Systems, vol. 34, no. 1, pp. 518–526, 2019.
[12] W. Du, Y. Wang, H. Wang, and Q. Fu, "Concept of modal repulsion for examining the sub-synchronous oscillations in power systems," IEEE Transactions on Power Systems, vol. 33, no. 4, pp. 4614–4624, 2018.
[13] F. L. Pagola, I. J. Perez-Arriaga, and G. C. Verghese, "On sensitivities, residues and participations: applications to oscillatory stability analysis and control," IEEE Transactions on Power Systems, vol. 4, no. 1, pp. 278–285, 1989.
[14] P. Kundur, Power system stability and control. McGraw-Hill Education, 1994.
[15] F. Wu and C. Desoer, "Global inverse function theorem," IEEE Transactions on Circuit Theory, vol. 19, no. 2, pp. 199–201, 1972.
[16] H.-W. Kim, S.-S. Kim, and H.-S. Ko, "Modeling and control of pmsg-based variable-speed wind turbine," Electric Power Systems Research, vol. 80, no. 1, pp. 46–52, 2010.
[17] J. Machowski, Z. Lubosny, J. W. Bialek, and J. R. Bumby, Power system dynamics: stability and control. John Wiley & Sons, 2020.
[18] Y. Liu, Q. H. Wu, H. Kang, and X. Zhou, "Switching power system stabilizer and its coordination for enhancement of multimachine power system stability," CSEE Journal of Power and Energy Systems, vol. 2, no. 2, pp. 98–106, 2016.
[19] W. Du, Z. Ma, Y. Wang, and H. F. Wang, "Harmonic oscillations in a grid-connected pv generation farm caused by increased number of parallel-connected pv generating units and damping control," CSEE Journal of Power and Energy Systems, pp. 1–9, 2020.
[20] L. Wang, S.-M. Lee, and C.-L. Huang, "Damping subsynchronous resonance using superconducting magnetic energy storage unit," IEEE transactions on energy conversion, vol. 9, no. 4, pp. 770–777, 1994.
[21] I. Dobson, J. Zhang, S. Greene, H. Engdahl, and P. W. Sauer, "Is modal resonance a precursor to power system oscillations," in International symposium on Bulk power System Dynamics and Control-IV Restructuring, Santorini, Greece. Citeseer, 1998, pp. 659–673.
[22] S. Li, T. A. Haskew, R. P. Swatloski, and W. Gathings, "Optimal and direct-current vector control of direct-driven pmsg wind turbines," IEEE Transactions on power electronics, vol. 27, no. 5, pp. 2325–2337, 2011.
[23] T. Knüppel, J. N. Nielsen, K. H. Jensen, A. Dixon, and J. Østergaard, "Small-signal stability of wind power system with full-load converter interfaced wind turbines," IET Renewable Power Generation, vol. 6, no. 2, pp. 79–91, 2012.
[24] J. Quintero, V. Vittal, G. T. Heydt, and H. Zhang, "The impact of increased penetration of converter control-based generators on power system modes of oscillation," IEEE Transactions on Power Systems, vol. 29, no. 5, pp. 2248–2256, 2014.
[25] S. Yazdani, M. Ferdowsi, and P. Shamsi, "Power synchronization pid control method for grid-connected voltage-source converters," in 2020 IEEE Kansas Power and Energy Conference (KPEC), 2020, pp. 1–6.
[26] L. Harnefors, "Analysis of subsynchronous torsional interaction with power electronic converters," IEEE Transactions on Power Systems, vol. 22, no. 1, pp. 305–313, 2007.
[27] D. Yang and V. Ajjarapu, "Critical eigenvalues tracing for power system analysis via continuation of invariant subspaces and projected arnoldi method," IEEE Transactions on Power Systems, vol. 22, no. 1, pp. 324–332, 2007.
[28] W. Du, X. Chen, and H. Wang, "A method of open-loop modal analysis to examine the ssos in a multi-machine power system with multiple variable-speed wind generators," IEEE Transactions on Power Systems, vol. 33, no. 4, pp. 4297–4307, 2018.
[29] ——, "Ssos caused by olmoc in a power system with the pmsgs for wind power generation," Renewable Power Generation, IET, vol. 12, no. 12, pp. 1405–1412, 2018.

Luonan Qiu received a B.E. degree in Energy Power and Mechanical Engineering from North China Electric Power University, Beijing, China, in 2017. She is currently pursuing the Ph.D degree in South China University of Technology. Her main research interests include power system stability analysis and control

Tianhao Wen received a B.E. degree in Electrical Engineering from Huazhong University of Science and Technology(HUST), Wuhan, China in 2018. He is currently pursuing the Ph.D degree in South China University of Technology. His research interests include nonlinear observers and power system transient stability analysis.

Yang Liu (CSEE: M'18, IEEE: M'18) received a B.E. degree and a Ph.D degree in Electrical Engineering from South China University of Technology (SCUT), Guangzhou, China, in 2012 and 2017, respectively. He is currently a Lecturer in the School of Electric Power Engineering, SCUT. His research interests include the areas of power system stability analysis and control, control of wind power generation systems, and nonlinear control theory. He has authored or co-authored more than 30 peer-reviewed SCI journal papers.

Q. H. Wu (CSEE: F'19, IEEE: M'91-SM'97-F'11) obtained a Ph.D. degree in Electrical Engineering from The Queen's University of Belfast (QUB), Belfast, U.K. in 1987. He worked as a Research Fellow and subsequently a Senior Research Fellow in QUB from 1987 to 1991. He joined the Department of Mathematical Sciences, Loughborough University, Loughborough, U.K. in 1991, as a Lecturer, subsequently he was appointed Senior Lecturer. In September, 1995, he joined The University of Liverpool, Liverpool, U.K. to take up his appointment to the Chair of Electrical Engineering in the Department of Electrical Engineering and Electronics. Currently, he is with the School of Electric Power Engineering, South China University of Technology, Guangzhou, China, as a Distinguished Professor and the Director of Energy Research Institute of the University. Professor Wu has authored and coauthored more than 600 technical publications, including 350 journal papers, 20 book chapters and 5 research monographs published by Springer. He is a Fellow of IEEE, Fellow of IET, Chartered Engineer and Fellow of InstMC. His research interests include nonlinear adaptive control, mathematical morphology, evolutionary computation, power quality and power system control and operation.